Journal of ELECTRONIC MATERIALS, Vol. 44, No. 2, 2015
DOI: 10.1007/s11664-014-3554-y
© 2014 The Minerals, Metals & Materials Society

Effect of an Al_2O_3/TiO_2 Passivation Layer on the Performance of Amorphous Zinc–Tin Oxide Thin-Film Transistors

DONG-SUK HAN,[1] JAE-HYUNG PARK,[1] MIN-SOO KANG,[1] SO-RA SHIN,[2] YEON-JAE JUNG,[2] DUCK-KYUN CHOI,[2] and JONG-WAN PARK[2,3]

1.—Department of Nanoscale Semiconductor Engineering, Hanyang University, 17 Haengdang-dong, Seoungdong-Ku, Seoul 133-791, Korea. 2.—Department of Materials Science and Engineering, Hanyang University, 17 Haengdang-dong, Seoungdong-Ku, Seoul 133-791, Korea. 3.—e-mail: jwpark@hanyang.ac.kr

The effect of an Al_2O_3/TiO_2 stacked passivation layer on the performance of amorphous ZnSnO (*a*-ZTO) thin-film transistors (TFTs) was investigated by comparing field-effect mobility (μ_{FE}) and subthreshold swing after passivation layer deposition. The values observed were 4.7 cm^2/Vs and 0.64 V/decade, respectively, for uncoated TFTs and 4.6 cm^2/Vs and 0.62 V/decade for passivated TFTs. In addition, excellent water vapor transmission was observed for electron beam-irradiated Al_2O_3/TiO_2-passivated poly(ether sulfone) substrates in a humidity test, because the Al_2O_3/TiO_2 passivation layer can enhance the interface properties between Al_2O_3 and TiO_2. To investigate the origin of this enhancement, we performed x-ray photoelectron spectroscopy of both unpassivated and Al_2O_3/TiO_2-passivated TFTs with *a*-ZTO back-channel layers after Ar annealing.

Key words: Amorphous oxide semiconductor, zinc-tin-oxide (ZTO), Al_2O_3/TiO_2, passivation layer, electron beam irradiation

INTRODUCTION

In recent years, ZnO-based amorphous oxide semiconductor (AOS) transparent thin-film transistors (TTFTs) have attracted much attention as feasible alternatives to covalently bonded semiconductors (e.g., *a*-Si or/and poly-Si TFTs) in next-generation flat panel display (FPD) applications. This remarkable development of oxide TFTs has been enabled by enhancement of high-mobility ZnO-based channel materials, resulting in a substantial amount of research in high-performance TFTs with oxide semiconductor active layers, for example InZnO (IZO),[1,2] ZnSnO (ZTO),[3,4] and InGaZnO (IGZO).[5–7] However, to achieve low-voltage consumption, improvements in subthreshold swing (*SS*) and field-effect mobility (μ_{FE}) are still required to meet the demands of integrated peripheral circuits on glass substrates. Recently, LG Display released a 55-in full-high-definition (FHD) organic light-emitting diode (OLED) TV containing an IGZO oxide TFT active matrix (AM).[8] Early in oxide semiconductor development, especially that of IGZO TFTs, field effect mobilities (μ_{FE}) of approximately 10 cm^2/Vs were regarded as sufficient for high-definition (HD) TV panels and higher-resolution mobile displays. However, recent trends in the flat panel display (FPD) industry have led to a drastic change to new phases, for instance, 4–8 K panels and three-dimensional (3D) displays. Thus, further improvements in μ_{FE} and in the stability of oxide TFT are required to increase potential applications.

The electrical performance of AOS-TFTs is strongly affected by interactions with the atmosphere. Jeong et al.[9,10] showed that the channel of IGZO TFTs is very sensitive to moisture adsorption. Thus, moisture permeation barrier films are necessary for long-term stability of oxide-based TFTs. Also, OLEDs are sensitive to moisture (H_2O) and oxygen (O_2), which can lead to device degradation, and should be protected from these species.[11] Simple calculations, primarily based on the degradation of the OLED cathode material when exposed to

(Received April 17, 2014; accepted November 24, 2014; published online December 10, 2014)

water vapor, suggest that the rate of permeation of water vapor must be less than 10^{-6} g/m^2/day to achieve a device lifetime of 10,000 h at room temperature. In FPD fabrication processes, such as AMLCD and AMOLED, a water vapor barrier film or encapsulation layer will also cover the TFT backplane. To date, a variety of organic or inorganic passivation layers, for example polymers, SiO_2, SiN_x, and Al_2O_3 have been studied.[12–16] It has been shown that surface roughness, chemical state, optical characteristics, and electrochemical properties can be manipulated by electron beam irradiation.[17,18] In this work, we deposited amorphous ZnSnO (a-ZTO) TFTs under optimum chamber conditions at room temperature by using a direct current (DC) magnetron sputtering system, and report a novel electron beam-irradiated Al_2O_3/TiO_2 passivation layer for use as a more reliable active channel layer. The effects of electron-beam treatment on the characteristics of Al_2O_3/TiO_2 permeability were then investigated. The permeability of the electron beam-irradiated Al_2O_3/TiO_2 thin films was studied with regard to their potential application as moisture barriers, and differences between physical and chemical characteristics before and after electron-beam treatment were investigated. Electron-beam-irradiated Al_2O_3 and TiO_2 thin films were then used as water vapor barrier films, and their suitability for stable ZTO-TFTs is discussed.

EXPERIMENTAL

Thin-Film Preparation

Figure 1a shows a schematic diagram of a cross-section of a bottom-gate a-ZTO TFT with a staggered structure. The devices were deposited on heavily doped n-type Si substrates coated with a buffered gate insulator (plasma-enhanced chemical vapor-deposited 10-nm SiO_2 layer/low pressure chemical vapor-deposited 100 nm SiN_x layer). A 20-nm-thick channel layer was grown by use of a DC magnetron sputtering system. A 4-inch-diameter target was placed 40 mm from the substrate, and a base pressure of 2.70×10^{-4} Pa, a working pressure of 6.67×10^{-1} Pa, and a plasma discharge power density of 0.5 W/cm^2 were used. The channel was patterned by using shadow masks with a channel length and a width-to-length ratio of 100 μm and 10:1, respectively. After source/drain (S/D) (Mo) electrode deposition, Al_2O_3 and TiO_2 barrier films were deposited by use of an electron cyclotron resonance (ECR) plasma-enhanced atomic layer deposition (PEALD) system. The barrier layer was etched by use of dilute HF solution for S/D contact. After deposition, the devices were annealed at 400°C for 60 min in ambient air. The precursors used in the PEALD of the Al_2O_3 and TiO_2 films were trimethylaluminium (TMA) and tetrakis(dimethylamino)titanium (TDMATi), respectively. The TMA and TDMATi sources were injected into the reaction chamber without a carrier gas. Injection times of the TMA, TDMATi, and O_2 plasma were fixed at 0.1, 1, and 10 s, respectively. The total cycle consisted of four steps to deposit the multilayer structure. The first and third step sequences consisted of TMA (0.1 s)/Ar (20 s)/O_2 plasma (10 s)/Ar (20 s) whereas the second and fourth steps included TDMATi (1 s)/Ar (20 s)/O_2 plasma (10 s)/Ar (20 s). Multilayer stacks with alternating Al_2O_3 and TiO_2 layers were deposited. To control the thickness of the Al_2O_3 and TiO_2 layers, the number of repeated cycles were varied. The TMA and TDMATi sources were maintained at 20°C by use of a cooling system and at 40°C by use of a heating system, respectively, and the base pressure inside the reactor was maintained at 13.3 Pa. Device structure was studied by use of high-resolution transmission electron microscopy. The channel layer had an amorphous structure, as shown in Fig. 1b. It was confirmed in the micrograph that the amorphous water vapor barrier film was well formed on the device. An electron cyclotron resonance (ECR) plasma was used for deposition of the water vapor barrier layers, because this plasma has a high density under low pressure; further, substrate damage because of ion bombardment is not a major concern because no electrode was present. The ECR plasma power and the deposition temperature were varied from 100 to 700 W and from 40°C to 100°C, respectively. To measure the water vapor transmission rate (WVTR) of the water vapor barrier films, 200-μm-thick 5×5 cm^2 polyethersulfone (PES) was used. Before deposition of the barrier films, the PES substrate was washed with isopropyl alcohol (IPA) and methanol in an ultrasonic bath before drying in a stream of nitrogen.

Electron Beam Irradiation

Al_2O_3/TiO_2 thin films were irradiated with an electron beam in different doses (1–100 kGy), by using an electron beam accelerator at the Korea Atomic Energy Research Institute (KAERI). The electron beam was generated by use of a potential of 1 MeV applied between the electron source and the sample target at room temperature. The distance between the source and sample was 400 mm, and the electron beam current was 1 mA. For comparison, a control sample was not subjected to irradiation with the electron beam.

Characterization and Measurement of Electrical Properties

After thin film deposition and electron beam irradiation, samples were subjected to more detailed analysis. Crystallinity change before and after electron beam irradiation was investigated by x-ray diffraction (XRD; Rigaku; D/max-2500), and the oxidation states of aluminium and titanium were determined by x-ray photoelectron spectroscopy (XPS; ESCA lab 220; VG Microtech). Film density change without and with electron-beam treatment were investigated by x-ray reflectometry (XRR,

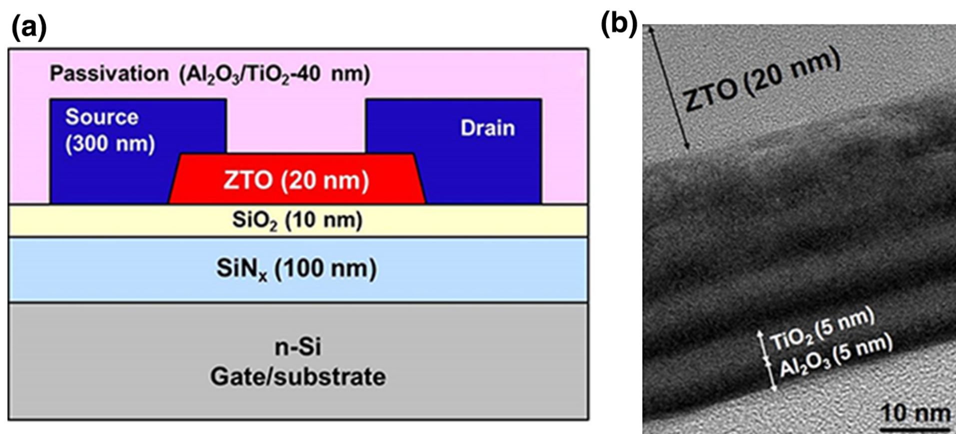

Fig. 1. (a) Schematic diagram of a cross-section of a bottom-gate-type HfZnSnO TFT with a staggered structure, and (b) TEM cross-sectional image of a HfZnSnO TFT with a quadruple stack of Al_2O_3/TiO_2 water vapor barrier film.

Panalytical X'pert Pro). The densities of the films were calculated from the XRR data by use of the equation[19]:

$$\theta_c = \lambda\sqrt{\left(\frac{\rho_e \gamma_e}{\pi}\right)} \quad (1)$$

when an x-ray beam is reflected at a grazing angle by a film, total external reflection of the radiation occurs below a critical angle. This critical angle, θ_c, can be approximated by using the above equation, where ρ_e is the electron density (the number of electrons per unit volume of the material), λ is the x-ray wavelength, and γ_e = 2.818 fm is the classical electron radius. The electron density calculated by use of the above equation can be transformed to reflect the density of the sample by using Avogadro's number, N_A, atomic weight, A, and the number of electrons per atom, Z, respectively.

Measurements of the WVTR were performed at 38°C and 100% RH by use of a Permatran W 3/33 (Modern Controls). All electrical characterization was performed by using a semiconductor property analyzer (Agilent HP 4145B) at room temperature in the dark.

RESULTS AND DISCUSSION

Water Vapor Passivation Layer Preparation

Figure 2 shows the dependence of the growth rate and density of Al_2O_3 and TiO_2 films on (a) substrate temperature, which was varied over a range of 32.5–102.5°C at a plasma power of 500 W, and (b) plasma power, which was varied over a range of 100–700 W at a substrate temperature of 80°C. The growth rate of Al_2O_3 and TiO_2 films decreased when the substrate temperature was increased from 32.5°C to 102.5°C. Al_2O_3 and TiO_2 film densities increased with increasing substrate temperature. In addition, the growth rate and density of the Al_2O_3 and TiO_2 films increased with plasma power until 700 W, at which they both decreased.

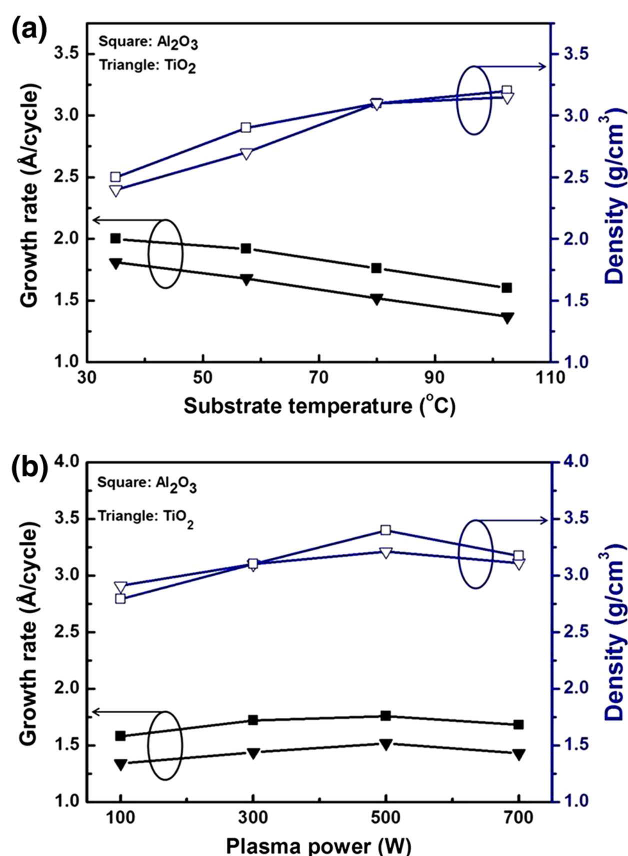

Fig. 2. Growth rate and thin film density of Al_2O_3 and TiO_2 as a function of (a) substrate temperature and (b) plasma power.

It was expected that the oxygen plasma reactant would be accompanied by energetic ion collision, resulting in plasma damage at a high plasma injection power. It was also expected that, when the density of the film increased, the WVTR value of the films would decrease slightly as the plasma power

increased.[20] Much work has focused on improving the properties of simple single-layer moisture barrier coatings; however, their qualities are not yet appropriate for application in next-generation FPD. Thus, to reinforce barrier characteristics, a four-pair Al_2O_3 (5 nm)/TiO_2 (5 nm) stacked approach was used to produce films with appropriate barrier qualities. The objective is to produce multilayers separated by an inorganic film to decouple the growth of defects between Al_2O_3 and TiO_2 layers. To examine the water vapor permeability characteristics of electron beam-irradiated Al_2O_3/TiO_2, WVTR measurements were performed. Figure 3 shows the WVTR as a function of electron beam dose for four different types of barrier film (Al_2O_3 (40 nm), TiO_2 (40 nm) single layer, double stack of Al_2O_3 (10 nm)/TiO_2 (10 nm), and quadruple stack of Al_2O_3 (5 nm)/TiO_2 (5 nm) layer) deposited on a PES substrate. To investigate the differences between single layer and multilayer (double stack or quadruple stack), single layer (Al_2O_3 and TiO_2) films, a double stack of Al_2O_3 (10 nm)/TiO_2 (10 nm) films and a quadruple stack of Al_2O_3 (5 nm)/TiO_2 (5 nm) films with a thickness of 40 nm were prepared. Compared with the bare PES film (50 g/m^{2}day), the TiO_2 and Al_2O_3 films had substantially improved WVTR. However, for a single layer, although the e-beam dose increased, the WVTR did not reach the detection limit of the typical permeability measurement system (5×10^{-3} g/m^{2}day). The most widely accepted value of the WVTR required for an OLED is 10^{-6} g/m^{2}day, so, a single-layer passivation film is not suitable for use on the active layers. On increasing the number of Al_2O_3/TiO_2 layers, the WVTR value was improved. Compared with the as-deposited water vapor barrier films, electron beam-treated films had enhanced WVTR values within the 10 kGy electron beam dose range. These results suggest that the WVTR of the barrier layer is improved by low-dose electron-beam treatment.

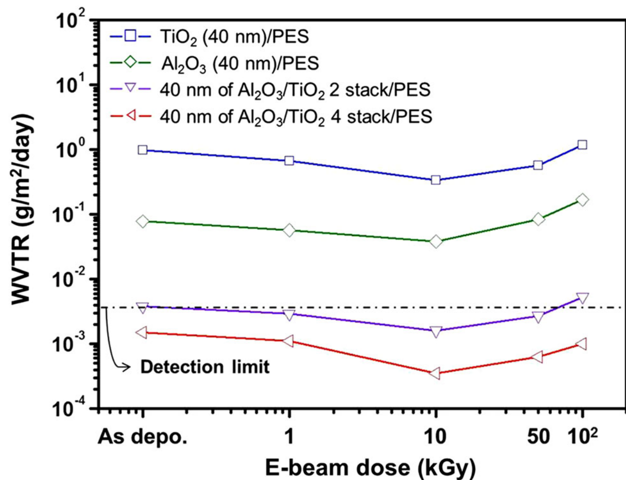

Fig. 3. WVTR values of the water vapor barrier films as a function of electron beam dose.

To examine the possible reason for the improved water vapor barrier characteristics of the Al_2O_3/TiO_2 films, XPS and XRD analysis was conducted. Figure 4a shows the oxygen deficiency ratio and the ratio of oxygen in water molecules adsorbed on the water vapor barrier films. The as-deposited film had a rather low oxygen deficiency ratio (<5%). However, with increasing e-beam dose, the oxygen deficiency ratio of the film increased slightly and the ratio varied from 3.5% to 10.2% with increases in the e-beam dose from 0 to 100. Similarly, the ratio of water molecules increased slightly with e-beam dose. The ratio varied from 2.6% to 6.3% as the e-beam dose increased from 0 to 100. Formation of an aluminate phase of Al_2O_3 and ZrO_2 in binary systems by alloying ZrO_2 and Al_2O_3 has been reported.[21] Similarly, it is expected that electron-beam treatment induced Al_2O_3/TiO_2 phase transformation from an amorphous to Al_2TiO_5 phase at the interface between the Al_2O_3 and TiO_2, as shown in Fig. 4b. Figure 4b shows XRD patterns for the 40-nm-thick quadruple stack of Al_2O_3 (5 nm)/TiO_2 (5 nm) films with increasing electron beam dose from 0 (as deposited) to 100 kGy. Amorphous films received sufficient energy for crystallization from a high electron beam dose. For this reason, a high dose electron beam caused Al_2TiO_5 crystallization at the interface, resulting in a large quantity of grain boundary in water vapor barrier layers.

Figure 5 shows a cross-sectional TEM image of an electron beam (100 kGy dose)-irradiated quadruple stack of Al_2O_3/TiO_2 on an a-ZTO surface. Al_2TiO_5 nanocrystal structures can be identified (for example, the one marked by arrows). It is important to note, however, that the nanocrystal extended far beyond the originating sublayer. The subsequent Al_2O_3 layer was amorphous, and thus contact with nanocrystals in neighboring Al_2TiO_5 sublayers could not be avoided. As a result, formation of highly efficient permeation paths, because of water vapor molecule diffusion along nanocrystal grain boundaries, accelerated. Figure 5 also shows that the interface between the Al_2O_3 and TiO_2 sublayers seems very smooth in the HRTEM image. Previous reports on similar structures of ZrO_2/Al_2O_3 laminates showed that formation of a $ZrAl_xO_y$-aluminate phase is thermodynamically favored compared with the separated ZrO_2/Al_2O_3 phase.[22] It is reasonable that a similar mixed phase forms at the sublayer boundaries in our Al_2O_3/TiO_2 multilayers. In a future study, this aluminate phase will be demonstrated (by characterization of its dielectric constant) to be denser than non-intermixed Al_2O_3/TiO_2 structures.

ZTO Thin Film Transistor Passivation

To investigate the relationships between moisture and TFT oxide characteristics, barrier films with four different structures were prepared on ZTO TFTs. The ZnO-to-SnO_2 molecular ratio in the ZTO

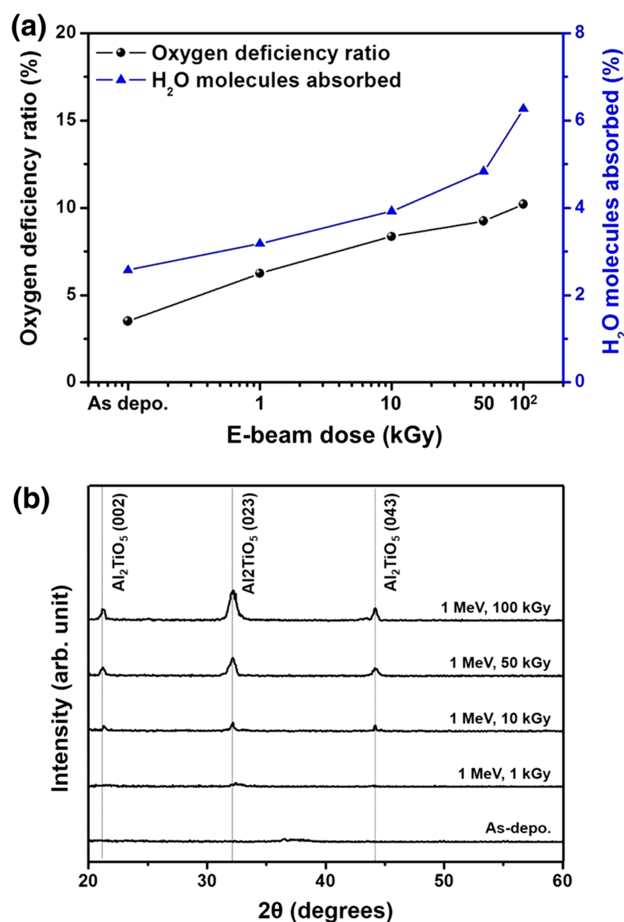

Fig. 4. (a) Ratio of oxygen in adsorbed water molecules (on the water vapor barrier films) to total oxygen and the oxygen deficiency ratio as a function of e-beam dose, (b) x-ray diffraction (XRD) patterns obtained from an electron beam-irradiated quadruple stack of Al_2O_3 (5 nm)/TiO_2 (5 nm) films.

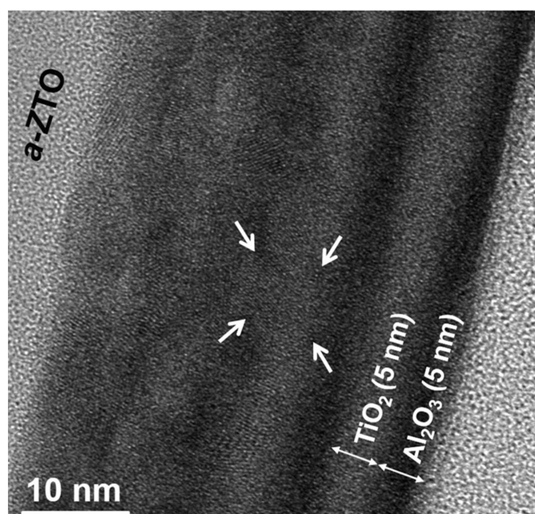

Fig. 5. TEM cross-sectional image of a quadruple stack of Al_2O_3/TiO_2 on an amorphous ZTO active layer after 1 MeV, 100 kGy electron beam irradiation. The arrows indicate Al_2TiO_5 nanocrystals.

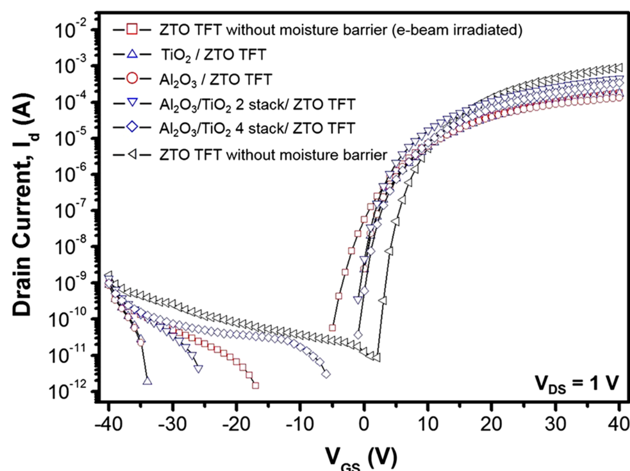

Fig. 6. Transfer characteristics of ZTO TFTs with different water vapor barrier layers. The devices were 1000 μm wide and 100 μm long, and V_{DS} = 1 V.

was 3:1. Figure 6 and Table I show the transfer curves and device properties, respectively, of the ZTO TFTs after deposition of the barrier films and annealing at 400°C. The apparent field-effect mobility, which is calculated as $\mu_{FE} = Lg_m/WC_iV_{DS}$, was extracted by using the transconductance measured at a low drain voltage ($V_{DS} \leq 1$ V), where W is the channel width, L is the channel length, C_i is the capacitance per unit area of the gate insulator, and g_m is the transconductance. The subthreshold swing (SS), defined as the voltage required to increase the source-to-drain current by a factor of 10, was calculated from $SS = dV_{GS}/d(\log I_{DS})$, where SS is the maximum slope in the transfer curve expressed on a log scale for $V_{GS} < V_{ON}$.

Possible explanations of the changes of the transfer characteristics of the TFTs were examined. The changes of the transfer characteristics, including μ_{FE} and SS, can be explained by:

1. Electron beam irradiation effects;
2. Plasma-induced damage; and
3. Ambient effects.

The field-effect mobilities (μ_{FE}) of the double stack and quadruple stack of Al_2O_3/TiO_2 barrier layer TFTs were comparable with each other and were higher than those of the other TFTs. The reduced mobilities of the TFTs without a barrier indicate that electron beam irradiation causes electronic collision in the ZTO channel layer. In general, μ_{FE} is affected by shallow traps near the conduction band, and the interaction of oxygen vacancies and zinc interstitials is an important source of n-type conductivity in ZnO-based materials.[23] During the electron beam irradiation process, electron beam-induced collision in the ZTO active channel layer increases trap sites at the top surface of the channel layer and thereby reduces mobility. Therefore, suppressing defect-related e-beam damage by

Table I. Comparison of the TFT device electrical properties: μ_{FE}, I_{On}/I_{Off}, SS, and V_{ON}

Channel layer	μ_{FE} (cm^2/Vs)	I_{On}/I_{Off}	SS (V/decade)	V_{On} (V)
ZTO TFT (without barrier or e-beam irradiation)	4.7	1.1×10^8	0.64	0
ZTO TFT (without barrier)	1.7	1.2×10^8	1.14	−6
ZTO TFT (TiO_2 40 nm)	1.7	9.6×10^7	1.09	−1
ZTO TFT (Al_2O_3 40 nm)	1.1	6.0×10^6	1.10	−1
ZTO TFT (double stack of Al_2O_3/TiO_2)	4.5	1.0×10^8	0.89	−2
ZTO TFT (quadruple stack of Al_2O_3/TiO_2)	3.6	1.1×10^8	0.82	−2

passivation layer deposition can effectively protect the channel layers. Also, SS values of the TFTs without a barrier layer were higher than those of the other devices. An increase in SS value can be attributed to the increase in total trap density in deep-level states in the channel layer, including the interface trap and bulk trap density.[24,25] Similar SS values for the TiO_2 and Al_2O_3 single-layer barrier TFTs suggest that an increase in the total trap density is caused not only by electron beam-induced collisions in the channel layer, but also plasma damage during the barrier-deposition process. Further, μ_{FE} and SS values of the ZTO TFT without a barrier or electron beam irradiation were higher and lower, respectively, than that of the TFT subjected to direct barrier deposition and electron beam irradiation. It is possible that the multilayer (double stack and quadruple stack of Al_2O_3/TiO_2) effectively prevented the plasma-induced damage and electron beam-induced bombardment that occurs during water vapor barrier deposition. These results indicate that ion-induced damage on the channel layer may be responsible for degradation of the TFT characteristics.

As mentioned above, the changes of the device characteristics μ_{FE} and SS can be attributed to interactions between the active backchannel and the ambient environment. It is well known that adsorbed oxygen/moisture can capture/release an electron, and the resulting absorbed species form a depletion/accumulation layer in the channel. Furthermore, water vapor adsorption involves trap creation in the channel layer, which is in contrast with oxygen adsorption.[9,10] The traps can be in either the shallow state or deep-level state in the forbidden bandgap of the oxide semiconductor. It is believed that an increase in the deep state trap density is the dominant mechanism causing degradation of the SS value. In addition, the traps created because of water vapor adsorption are in the deep-level state. However, the major effects of device degradation under plasma-induced ion damage, ambient effects, or electron beam bombardment are still not completely understood. In future work, electron beam irradiation and plasma ion damage effects will be discussed in terms of activation energy for E_F-conducting measurements and bias temperature stability. In this discussion, our multilayers (electron beam-irradiated double and quadruple stacks of Al_2O_3/TiO_2) are expected to be beneficial to further suppression of moisture permeation through the barrier stack. The apparent result is passivation layers with both a low permeation rate for water and a very low density of Al_2O_3/TiO_2 interface boundaries, enabling highly efficient sealing of large-area display devices.

CONCLUSIONS

In summary, PEALD-deposited Al_2O_3/TiO_2 water vapor barrier films were treated with different doses of electron beam irradiation, and ZTO-TFTs were applied to these electron beam-irradiated barrier films. Crystallinity, oxidation state, and WVTR were remarkably modified by electron beam irradiation and were found to be strongly dependent on electron beam dose.

By optimizing the electron beam irradiation conditions, device properties were improved, as were the ZTO TFT field-effect mobility (μ_{FE}) and subthreshold swing (SS) values. It was shown that performance degradation was only to because of ambient effects but also dynamic interactions between the exposed backchannel and electron beam irradiation. Therefore, a suitable barrier layer with the lowest WVTR is essential to improve the performance of ZTO TFTs.

ACKNOWLEDGEMENTS

This research was supported by the Basic Science Research Program through the National Research Foundation of Korea (NRF) funded by the Ministry of Education (NRF-2012M2B2A4029342).

REFERENCES

1. P. Barquinha, P. Ferreira, L. Pereira, G. Goncalves, and E. Fortunato, *J. Appl. Phys.* 101, 044505 (2007).
2. K.B. Park, J.B. Seon, G.H. Kim, M. Yang, B. Koo, H.J. Kim, M.K. Ryu, and S.Y. Lee, *IEEE Electron Dev. Lett.* 31, 311 (2010).
3. Y.S. Rim, D.L. Kim, W.H. Jeong, and H.J. Kim, *Electrochem. Solid-State Lett.* 15, H37 (2012).
4. P.K. Nayak, M.N. Hedhill, D. Cha, and H.N. Alshareef, *ACS Appl. Mater. Interfaces.* 5, 3587 (2013).
5. J. Lee, D. Kim, D. Yang, S. Hong, K. Yoon, P. Hong, C. Jeong, H. Park, S.Y. Kim, and S.L. Lim, *Proceedings of the SID'08 Digest* (2008), p. 625.

6. J.K. Jeong, J.H. Jeong, H.W. Yang, T.K. Ahn, M. Kim, K.S. Kim, B.S. Gu, H.-J. Chung, J.-S. Park, and Y.-G. Mo, *J. Soc. Inf. Disp.* 17, 95 (2009).
7. E. Chong, Y.W. Jeon, Y.S. Chun, D.H. Kim, and S.Y. Lee, *Thin Solid Films* 519, 4347 (2011).
8. C.W. Han, K.M. Kim, S.J. Bae, H.S. Choi, J.M. Lee, T.S. Kim, Y.H. Tak, S.Y. Cha, and B.C. Ahn, *SID Int. Symp. Digest Tech. Papers* (2012), p. 279.
9. J.K. Jeong, H.W. Yang, J.H. Jeong, Y.-G. Mo, and H.D. Kim, *Appl. Phys. Lett.* 93, 123508 (2008).
10. J.-S. Park, J.K. Jeong, H.-J. Chung, Y.-G. Mo, and H.D. Kim, *Appl. Phys. Lett.* 92, 072104 (2008).
11. P.E. Burrows, V. Bulovic, S.R. Forrest, L.S. Sapochack, D.M. McCarty, and M.E. Thompson, *Appl. Phys. Lett.* 65, 2922 (1994).
12. M. Fakhri, N. Babin, A. Behrendt, T. Jakob, P. Görrn, and T. Riedl, *Adv. Mater.* 25, 2821 (2013).
13. S.-M. Seo, C.-H. Jang, and J.-H. Park, *Org. Electron.* 9, 899 (2008).
14. M. Kim, J.H. Jeong, H.J. Lee, T.K. Ahn, H.S. Shin, J.-S. Park, J.K. Jeong, Y.-G. Mo, and H.D. Kim, *Appl. Phys. Lett.* 90, 212114 (2007).
15. Y. Liu, H. Wang, and K. Radhakrishman, *Thin Solid Films* 515, 4387 (2007).
16. M.D. Groner, S.M. George, R.S. McLean, and P.F. Carcia, *Appl. Phys. Lett.* 88, 051907 (2006).
17. X.G. Hou and A.D. Liu, *Rad. Phys. Chem.* 77, 345 (2008).
18. J. Chen, M. Czayka, and R.M. Uribe, *Rad. Phys. Chem.* 74, 31 (2005).
19. W. Wu, W.E. Wallace, E.K. Lin, G.W. Lynn, C.J. Glinka, E.T. Ryan, and H. Ho, *J. Appl. Phys.* 87, 1193 (2000).
20. W.S. Kim, M.-G. Ko, T.-S. Kim, S.-K. Park, Y.-K. Moon, S.-H. Lee, J.-G. Park, and J.-W. Park, *J. Nanosci. Nanotechnol.* 8, 4726 (2008).
21. J. Meyer, H. Schmidt, W. Kowalsky, T. Riedl, and A. Kahn, *Appl. Phys. Lett.* 96, 243308 (2010).
22. C. Zhao, O. Richard, H. Bender, M. Caymax, S. De Gendt, M. Heyns, E. Young, G. Roebben, O. Van Der Biest, and S. Haukka, *Appl. Phys. Lett.* 80, 2374 (2002).
23. Y.-S. Kim and C.H. Park, *Phys. Rev. Lett.* 102, 086403 (2009).
24. M.K. Ryu, S. Yang, S.-H. Ko Park, C.-S. Hwang, and J.K. Jeong, *Appl. Phys. Lett.* 95, 072104 (2009).
25. D.W. Greve, *Field Effect Devices and Application: Devices for Portable, Low power, and Imaging Systems*, 1st ed. (Englewood Cliffs: Prentice-Hall, 1998).